

MICROANALYTICAL CHARACTERIZATION OF SLAGGING DEPOSITS IN A PILOT-SCALE COMBUSTOR

J. West and J.N. Harb
Department of Chemical Engineering and
Advanced Combustion Research Center
Brigham Young University
Provo, Utah 84602

Keywords: Slagging, coal ash deposits, SEMPC

INTRODUCTION

The purpose of this work was to characterize a set of deposit samples with respect to their compositions, phases present, and morphology. An understanding of how these properties change as a deposit grows is essential to developing a physical picture of deposit behavior, especially transitions in behavior from heterogeneous agglomerations of particles to highly sintered particles, or even a completely homogeneous molten phase that assimilates all impacting particles. Indeed, these deposit properties are of primary importance in determining the effect of deposition on heat transfer through the water wall, and on the removability of the deposit. These properties must be understood and quantified in order to predict deposition behavior.

ANALYSIS PROCEDURE

Analyses were performed on two water-wall samples from ABB-CE's Fireside Performance Test Facility (FPTF), a pilot-scale facility which operates at temperatures, heat fluxes and residence times representative of those found in full-scale units [1]. Both deposit samples were formed while firing the same U.S. Eastern Bituminous coal. The samples were cross-sectioned and prepared for analysis in a Scanning Electron Microscope (SEM). An ISIS microanalytical system equipped with X-ray and backscatter detectors was used to run a Scanning Electron Microscopy Point Counting (SEMPC) analysis [2] to determine elemental compositions at discrete points on the sample. Backscattered electron (BSE) images were also collected and evaluated, in which the brightness of a point is proportional to the atomic number of the species present at that point. Thus, in BSE images of these samples, regions with heavy elements such as iron are bright white, aluminosilicates are light grey, silicates are dark grey, and the epoxy mounting medium is black.

An important consideration in this work is the changes in deposit properties as the deposits grows, or increases in thickness. Thus, the samples analyzed were cross-sectioned, and analyses of these samples were conducted in 10-12 discrete regions of the deposit, from the initial layer to the outer region of the deposit. Since it is not possible in this forum to discuss each of the regions individually, we have chosen to discuss three regions representative of the changes taking place. Of particular interest in this study is the transition from 'inner layer' behavior to the strongly sintered outer layer, since this transition is often the one that leads to formation of tenacious or otherwise troublesome slagging deposits [3].

RESULTS AND DISCUSSION

Changes in morphology of the deposit samples provide an excellent framework from which to understand changes in other deposit properties and behavior. Figures 1, 2, and 3 are BSE images of three distinct regions of the deposit, referred to as the inner layer, intermediate region, and outer region, respectively. Both of the samples analyzed showed dramatic changes in morphology through the deposit in the direction of deposit growth. Figure 1 shows the morphology of the initial layer, which can be characterized by its small particle size and discrete and spherical particles. Immediately next to the initial layer, the particles become larger and less round and regular in shape and appearance. The intermediate region occurs as the particles show signs of sintering and/or agglomeration, as shown in Fig. 2. However, discrete Fe-rich and Si-rich particles are still evident throughout this region of the deposit. Next there occurs, in gradual increments, the increased sintering and assimilation of particles, culminating in a largely homogeneous phase at the outer region where crystallization can be observed (Fig. 3).

These changes in morphology are strongly connected to changes in the elemental and phase

compositions throughout the deposit. Figure 4 shows a triangular histogram of the compositions of Fe, Al and Si in the initial layer of the deposit, which has been normalized to elemental mole percents (not oxides). It can be seen that the bulk of the particles are kaolinite-type aluminosilicates with an Al/Si ratio of approximately one and a small amount of Fe. There are also significant amounts of Fe-rich and Si-rich particles present. Figure 5 is a ternary diagram which corresponds to the intermediate region of the deposit (Fig. 2). In this region, the deposit is heterogeneous. The number of Fe-rich and Si-rich particles has begun to decrease due to mixing with the aluminosilicate phases, resulting in the overall broadening of the range of compositions toward more Fe and Si-rich aluminosilicates. Note that the compositions are spread over a much wider region than in the initial layer. The heterogeneity is an indication of local assimilation of Fe-rich and Si-rich particles. At the outer region of the deposit, the compositions form into a more narrow band as the deposit becomes more homogeneous. A small increase in Al-rich aluminosilicates ($Al/Si > 1$) is also observed, corresponding to the crystallization of mullite ($3(Al_2O_3)2(SiO_2)$) in the deposit.

In the samples studied, K was deposited selectively in the inner layer of the deposit. Table 1 shows the bulk elemental compositions from each of the regions analyzed, from inner to outer regions; the amount of K_2O present in the initial layer is significantly higher than that found in the deposit regions further from the wall. It should also be noted from Table 1 that, other than the initial layer, the bulk concentration remains largely constant throughout all regions of the deposit. Therefore, it is the phase distribution that changes in different regions of the deposit rather than the elemental composition.

Analysis of the distribution of K in the deposit phases shows that the amount of particles with more than 3 mole % of K decreased dramatically from the initial layer to the intermediate region of the deposit. This shift occurred as the potassium aluminosilicate particles were assimilated into other aluminosilicates. This assimilation tends to decrease the melting temperature of the resulting mixture, facilitating the assimilation of other particles and resulting in an increase in cluster size. Therefore, K-aluminosilicates played a significant role in the transition from the inner layer to the intermediate layer.

Although the elemental percent of Fe was relatively constant throughout the deposit (Table 1), the phases in which it was found changed significantly. The distribution of Fe-containing particles in the inner layer showed the presence of some Fe-aluminosilicates with relatively high amounts of iron (>10 mole %). These particles, presumably formed by coalescence of aluminosilicates and Fe-rich minerals in the coal, appeared to be assimilated early (just outside the inner layer). Iron assimilation appeared to be localized in the intermediate region of the deposit. In contrast, the iron content was much more homogeneous in the outer regions of the deposit.

CONCLUSIONS

For the coal and combustor system analyzed, the results indicate that both K and Fe have significant effects on deposition behavior in the early deposition stage. Both K and Fe act to accelerate the sintering and melting behavior of the aluminosilicates which make up the bulk of the deposit. In particular, Fe played an important role throughout the deposit, and its distribution was indicative of the extent of homogeneity of the deposit.

Through detailed microanalytical characterization of deposits from a combustor representative of a utility boiler, we have shown the presence of inherently different and distinct regions of the deposit. The transitions between these regions are the key to determining when undesirable deposit behavior is likely to occur, and are also important to determining the mechanisms which determine deposit behavior and properties in each region. Additional work is needed in this area to enhance the ability to quantify deposit behavior and properties at all stages of deposit growth and to develop mechanisms which can be applied in mathematical models to predict deposition behavior.

ACKNOWLEDGMENTS

This work was sponsored by the Advanced Combustion Engineering Research Center. Funds for this Center are received from the National Science Foundation, the State of Utah, 42 industrial participants, and the U.S. Department of Energy. We wish to thank ABB-CE for providing the samples from their FPTF.

REFERENCES

- [1] Combustion Engineering, "Developing a Coal Quality Expert: Combustion and Fireside Performance Characterization Factors," Progress Report, July 1992.
- [2] Jones, M.L., Kalmanovitch, D.P., Steadman, E.N., Zygarlicke, C.J., and Benson, S.A., "Application of SEM Techniques to the Characterization of Coal and Coal Ash Products" in H.L.C. Meuzelaar (Ed.), *Advances in Coal Spectroscopy*, Plenum Press, New York, 1991.
- [3] Wain, T.F., Livingston, W.R., Sanyal, A., and Williamson, J., "Thermal and Mechanical Properties of Boiler Slags of Relevance to Sootblowing," in S.A. Benson (Ed.), *Inorganic Transformations and Ash Deposition During Combustion*, United Engineering Trustees, Inc., New York, 1992.

Table 1: Selected bulk elemental compositions at regions throughout the deposit (oxide mole %). Region numbers begin at the initial layer and increase through the outer region.

Region No.	Al ₂ O ₃	SiO ₂	K ₂ O	CaO	TiO ₂	Fe ₂ O ₃
1	34.66	50.77	3.27	1.49	1.56	6.21
2	33.37	55.9	2.13	1.24	1.6	4.65
3	33.23	53.36	1.91	2.09	1.66	6.97
4	32.85	56.36	1.59	1.64	1.48	5.57
5	31.51	56.52	1.65	1.68	1.44	6.64
6	31.77	56.92	1.68	1.36	1.45	6.28
7	32.69	56.18	1.57	1.38	1.73	5.91
8	30.96	58.35	1.44	1.31	1.5	5.85
9	31.08	56.94	1.66	1.37	1.39	7.03
10	27.96	52.56	1.33	1.4	1.24	7.85
11	30.71	57.42	1.66	1.35	1.31	7.08
12	30.75	57.67	1.74	1.5	1.47	6.43
13	31.84	56.47	1.69	1.52	1.45	6.63

Figure 1. BSE image of the initial layer of the deposit (600x).

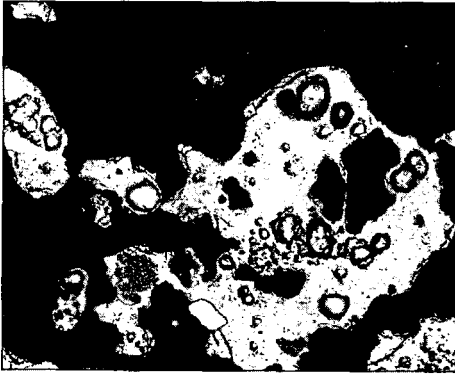
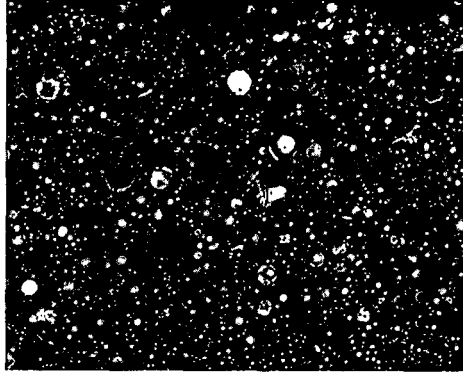


Figure 2. BSE image of the intermediate region of the deposit (300x).

Figure 3. BSE image of the outer region of the deposit (300x).



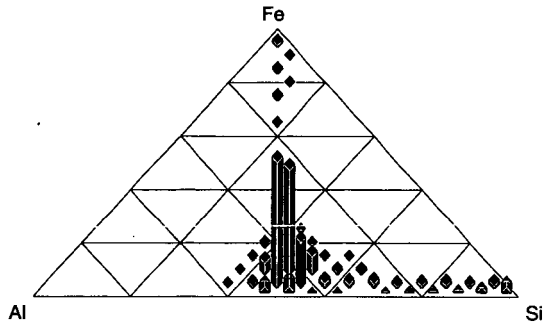


Figure 4. Frequency distribution of compositions found in the initial layer of the deposit (mole %).

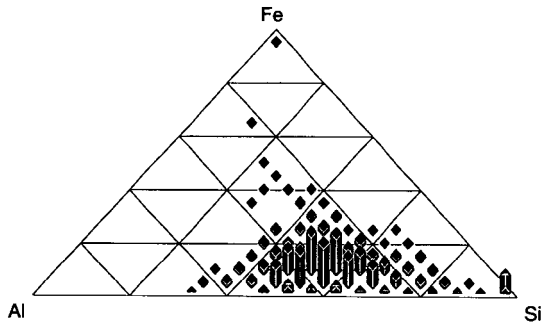


Figure 5. Frequency distribution of compositions found in the intermediate region of the deposit (mole %).

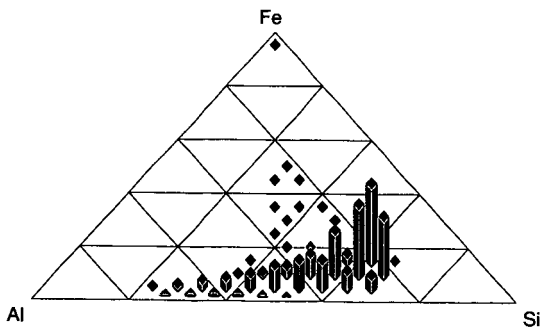


Figure 6. Frequency distribution of compositions found in the outer region of the deposit (mole %).